Potential Major Improvement in Superconductors for High-Field Magnets

Jamil Tahir-Kheli,[1] Tomáš Hlásek,[2,3] Michal Lojka,[3,2] Michael S. Osofsky,[4] and Carver A. Mead[1]

[1] *Engineering & Applied Science, California Institute of Technology, Pasadena, CA 91125, USA*
[2] *CAN SUPERCONDUCTORS, s.r.o., Ringhofferova 66, 251 68 Kamenice, Czech Republic*
[3] *Department of Inorganic Chemistry, University of Chemistry and Technology Prague, Technická 5, 166 28, Prague 6, Czech Republic*
[4] *Department of Physics, Astronomy & Geosciences, Towson University, 8000 York Road, Towson, MD 21252, USA*
https://arxiv.org/abs/2304.06171

Fusion reactors are limited by the magnetic field available to confine their plasma. The commercial fusion industry uses the larger magnetic field and higher operating temperature of the cuprate superconductor $YBa_2Cu_3O_{7-\delta}$ (YBCO) in order to confine their plasma into a dense volume. A superconductor is a macroscopic quantum state that is protected from the metallic (resistive) state by an energy gap. Unfortunately, YBCO has an anisotropic gap, known as D-wave because it has the shape of a $d_{x^2-y^2}$ chemical orbital. This D-wave gap means that poly-crystalline wire cannot be made because a few degree misalignment between grains in the wire leads to a drastic loss in its supercurrent carrying ability, and thereby its magnetic field limit. The superconductor industry has responded by growing nearly-single-crystal superconducting YBCO films on carefully prepared substrate tapes kilometers in length. Heroic development programs have made such tapes commercially available, but they are very expensive and delicate. MRI magnet superconductors, such as NbTi and Nb_3Sn, are formed into poly-crystalline wires because they have an isotropic gap in the shape of an s chemical orbital (called S-wave) that makes them insensitive to grain misalignment. However, these materials are limited to lower magnetic fields and liquid-He temperatures. Here, we modified YBCO by doping the Y site with Ca and Ce atoms to form $(Y_{1-x-y}Ca_xCe_y)Ba_2Cu_3O_{7-\delta}$, and show evidence that it changes to an S-wave gap. Its superconducting transition temperature, T_c, of $\sim$ 70K, while lower than that of D-wave YBCO at $\sim$ 90K, is easily maintained using common, economic cryogenic equipment.

In the popular press, T_c is considered the most important figure-of-merit of a superconductor. This line of thinking assumes that a higher T_c always leads to better technology because the main obstacle is the cooling cost. In fact, the maximum sustainable magnetic field at the operating temperature and the cost and reliability of making kilometers of wire are far more important for current and near-future technologies [1]. Since YBCO can sustain higher magnetic fields at higher temperatures than NbTi or Nb_3Sn, the biggest problem with YBCO is making long wires. Thus a natural question to ask is, "Can we lower the T_c of D-wave YBCO in order to expose an S-wave YBCO gap phase that will intrinsically perform better when made into poly-crystalline wires?"

It is known [2] that non-magnetic impurities smear out the superconducting gap anisotropy. For a D-wave superconductor, this gap smearing reduces its gap anisotropy, and thereby its T_c [3]. Smearing an isotropic gap has no affect on the overall gap isotropy. Thus, non-magnetic impurities do not affect the T_c of S-wave superconductors [4]. Hence, the plan in this paper is to add sufficient non-magnetic impurities to YBCO such that the D-wave T_c becomes smaller than the S-wave T_c.

Figure 1 shows the two possible scenarios for the S-wave T_c of YBCO relative to its D-wave T_c. Figure 1a is the consensus expectation that the S-wave T_c is so small such that, if ever uncovered, it would be practically useless due to cooling costs. Figure 1b is our conjecture for where the S-wave T_c is located [5]. If Figure 1b is true, then there is enormous value to current magnet technologies in uncovering this S-wave phase of YBCO.

To decide between Figure 1a and Figure 1b, three experiments were performed on YBCO samples with different concentrations of non-magnetic impurities. Each experiment was chosen because it analyzed a distinct fundamental physical characteristic of the superconducting gap.

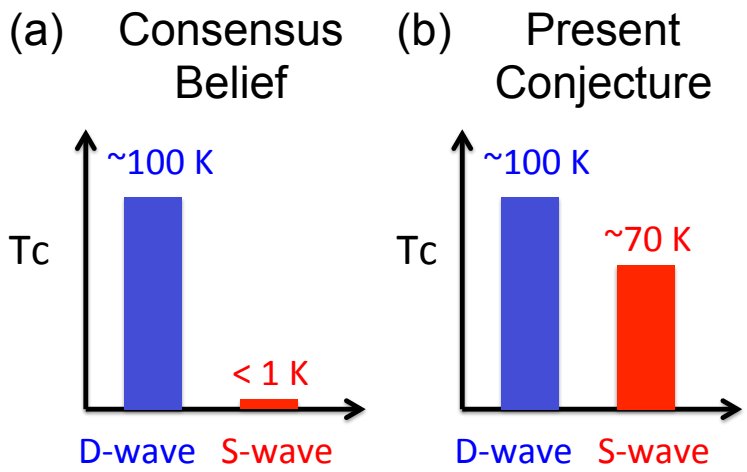

Fig. 1 | Is a technologically useful YBCO S-wave superconductor hiding just below the difficult to manage D-wave YBCO? (a) shows the consensus belief that any S-wave YBCO phase would have its T_c below 1 K, and thus would not be a useful technology. (b) shows our conjecture that an S-wave phase in YBCO exists at $\sim$ 70 K. If true, unearthing this phase would have huge implications for high-magnetic-field applications. Here, we tried to "push down" the D-wave phase T_c, while not affecting the S-wave phase T_c. Our approach is to add non-magnetic Ca and Ce atoms to $YBa_2Cu_3O_{7-\delta}$ to form $(Y_{1-x-y}Ca_xCe_y)Ba_2Cu_3O_{7-\delta}$ [hereinafter, denoted by (X,Y)]. Our experimental results are shown in Figures 2, 3, and 4. Table I summarizes the results. Taken together, they suggest that an S-wave YBCO phase does exist at $\sim$ 70 K.

I. THREE EXPERIMENTS TO DISTINGUISH BETWEEN D-WAVE AND S-WAVE GAP SYMMETRIES

The superconducting gap is represented by a complex number that is a function of direction with respect to the crystal axes of YBCO. It has magnitude and phase in every direction. The gap is invariant to an overall phase change. The T_c is proportional to the maximum magnitude of the gap. For S-wave and D-wave gap symmetries, the gap function can be taken to be real in every direction. An S-wave gap is positive, while a D-wave gap is positive and negative with a zero in-between. The D-wave gap in YBCO has zeros, or nodes, along directions 45° from the axes along the Cu-O bond directions in the CuO_2 planes and opposite signs along the two perpendicular Cu-O bond directions.

As described above, the T_c of D-wave YBCO should fall with increasing non-magneic impurities while the T_c of an S-wave YBCO phase should remain approximately constant with varying impurity concentrations. The first experiment measures the T_c evolution with impurity concentration. The results of the experiment are shown in Figure 2 with additional details of the experiment below.

The second experiment looks for the existence of a sign change in the gap in order to distinguish a D-wave gap from and S-wave gap. A D-wave gap leads to a zero-bias conductance peak (ZBCP) in Point-Contact-Andreev-Reflection (PCAR) tunneling current, while an S-wave gap has no ZBCP. The results of this experiment are shown in Figure 3 with additional details below.

The third experiment searches for nodes in the superconducting gap by measuring the evolution of the superconducting penetration depth, λ as a function of temperature, T, at low-temperatures. A D-wave gap has nodes and will lead to $\lambda \sim T$, and an S-wave gap leads to $\lambda \sim T^2$ because it has no nodes [6]. The results of this experiment are shown in Figure 4 with additional details below.

The non-magnetic impurities used in this paper are Ca atoms that substitute at the Y sites in a +2 oxidation state, and Ce atom that substitute at the Y site in a +4 oxidation state. Both of these atoms are non-magnetic. Since the oxidation state of Y in YBCO is +3, Ca and Ce have a −1 and +1 charge relative to the Y atoms, respectively. Also, the ionic radii of Ca (+2), Ce (+4), and Y (+3) are very close. They are 1.00 Å, 1.11 Å, and 1.02 Å, respectively. Thus Ca and Ce atoms do not strain YBCO. This Ca and Ce charge "counter-doping" has the benefit of permitting very large amounts of non-magnetic dopants to substitute at the Y site. Large doping is desirable since we want to push the D-wave T_c down as far as possible in order to increase our chances of unearthing the S-wave gap phase.

There were many other potential non-magnetic atoms. We chose Ca and Ce because they both substitute at the Y site of YBCO, Ca-doped YBCO is a superconductor [7, 8], and Ce-doped YBCO is also a superconductor [9]. For both Ca and Ce doping, the T_c is only modestly lower than pure YBCO.

Samples of $(Y_{1-x-y}Ca_xCe_y)Ba_2Cu_3O_{7-\delta}$ [hereinafter, denoted by (X,Y)] for (X,Y) = (0.0, 0.0), (0.13, 0.0), (0.13, 0.13), (0.26, 0.13), (0.32, 0.16), (0.36, 0.16), (0.26, 0.26), (0.29, 0.29), and (0.32, 0.32) were synthesized. Since pure YBCO, $(0, 0)$ in our notation, has a superconducting T_c dome that rises from zero, peaks, and then decreases as the number of Oxygen atoms in the CuO chains increases, we expect that all (X,Y) samples will have similar T_c domes [10].

Many low-temperature anneals were done on each sample to change the Oxygen content and thereby obtain the maximum T_c, ($T_{c,max}$) value for each (X,Y) for all samples reported in this paper. Extended Data Figures 1, 2, 3, and Extended Data Tables II and III are materials characterization data that show the samples are single-phase with the stated composition.

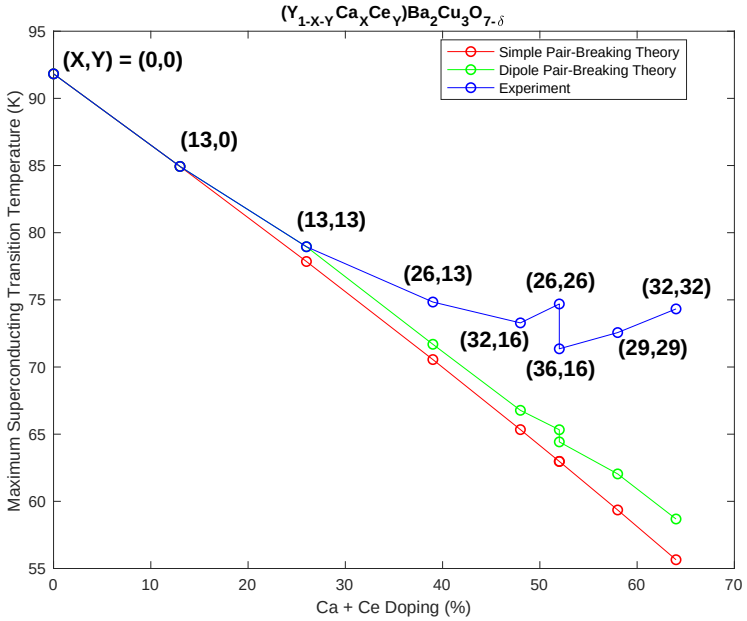

Fig. 2 | Evolution of the maximum superconducting $T_{c,max}$ *vs* Ca and Ce counter-doping in YBCO compared to D-wave theory predictions. Blue points are $T_{c,max}$ which initially drops with counter-doping and then "saturates" at ∼ 72 K. Saturation of $T_{c,max}$ suggests the known D-wave of pure YBCO has changed to S-wave because the T_c of S-wave superconductors is only weakly dependent on non-magnetic counter-doping [4] (Anderson's Theorem). $T_{c,max}$ is the maximum T_c for each (X, Y) after low-temperature annealing that changes the Oxygen content of the sample. Red and green points are the predicted $T_{c,max}$ results. Red points assume simple pair-breaking, where Ca and Ce atoms lead to identical pair-breaking strengths. Green points assume that Ca and Ce atoms are close together in the material because Ca and Ce have +1 and −1 charges relative to Y, respectively (hence, the name "dipole pair-breaking"). Details are given in the Supplement [11]. The red and green points do not explain the experiment (blue points) suggesting that highly counter-doped YBCO is an S-wave superconductor.

A. Evolution of the maximum T_c with impurity concentration

Figure 2 shows the maximum superconducting $T_{c,max}$ as a function of (X,Y) counter-doping. It shows that $T_{c,max}$ initially falls, as expected for a D-wave superconductor, and then "saturates" at higher doping. The red and green plots are the results of two different theoretical models, using Abrikosov-Gorkov theory [2, 3], for the drop in T_c versus counter-doping if all the samples remained D-wave [11]. The saturation of the measured $T_{c,max}$ (blue points) is not compatible with D-wave superconductivity predictions and suggests that highly counter-doped YBCO is an S-wave superconductor.

A very important detail of this experiment is that the maximum T_c for each counter-doping was used. Tallon et al. [12, 13] showed that the T_c dome of cuprate superconductors corresponds to the hole doping in the CuO_2 planes and that this hole doping leads to a unique room-temperature thermopower. From these two relations, $T_{c,max}$ is predicted to occur when the room-temperature thermopower is $\approx +2$ μV/K. For all (X,Y) values, this relation was found to be true. We conclude that for each (X,Y), the number of holes in the CuO_2 planes is the same when the transition temperature is maximum. Therefore, any change in $T_{c,max}$ as a function of (X,Y) is not due to changes in the Fermi level, Fermi surface, or hole doping in the CuO_2 planes.

B. Evolution of a zero-bias-conductance peak in Point-Contact-Andreev-Reflection

The second experiment looked for a sign change in the superconducting gap using Point-Contact-Andreev-Reflection [14] (PCAR). PCAR measures the tunneling current from a normal metal (in this case Cu) point contact into the superconductor. The normal metal has a continuum of states in the neighborhood of the Fermi level, whereas the superconductor has its energy gap centered on its Fermi level. Thus no normal current can tunnel from the normal level into the superconductor for bias voltages less than half the gap. However, there are normal states in a D-wave superconductor in the regions where its gap changes sign, and electrons from the normal metal tip can tunnel into these states, thereby showing a sharp peak near zero bias voltage, known as the zero-bias conductance peak (ZBCP) [15, 16]. An S-wave gap has no sign change and hence no ZBCP in PCAR. See Figure 3.

The figures shows representative conductance plots from many spectra for $(0, 0)$ and $(0.32, 0.32)$. Since $(0, 0)$, pure YBCO, is D-wave, a ZBCP is seen, as expected. For heavily counter-doped $(0.32, 0.32)$, no ZBCP was found. We conclude that PCAR suggests highly counter-doped YBCO is an S-wave superconductor.

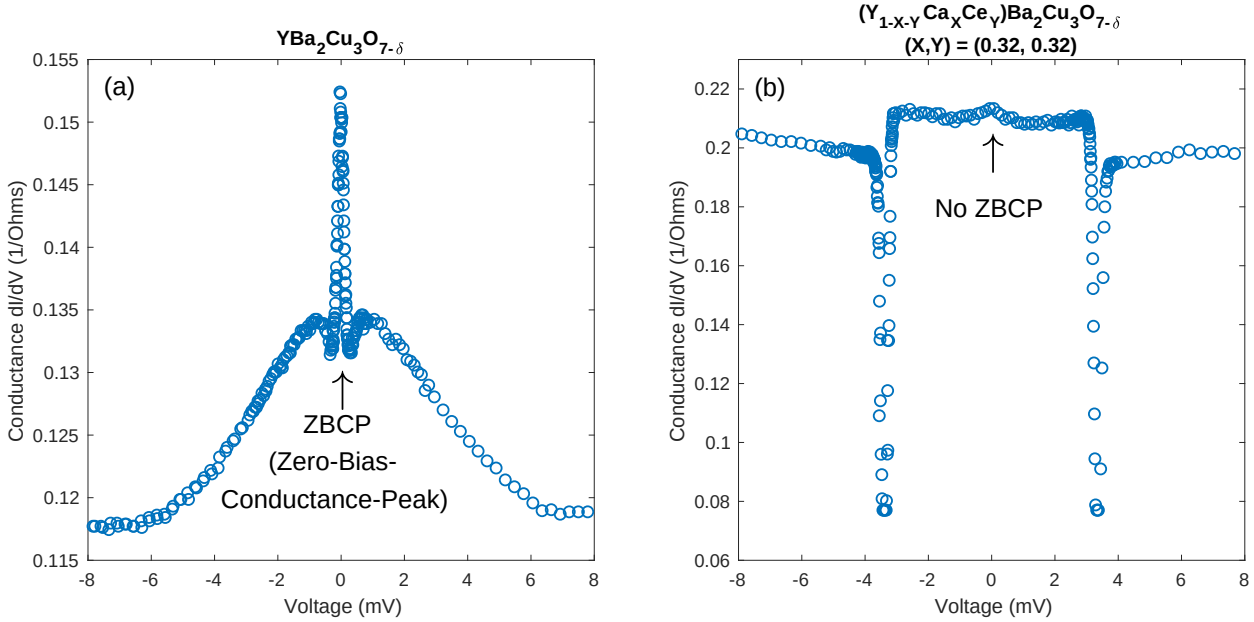

Fig. 3 | Point-Contact-Andreev-Reflection [20] (PCAR) on pure YBCO, or $(\mathbf{X}, \mathbf{Y}) = (\mathbf{0}, \mathbf{0})$, and $(\mathbf{X}, \mathbf{Y}) = (\mathbf{0.32}, \mathbf{0.32})$. A ZBCP in PCAR is a signature of a D-wave phase. No ZBCP is expected for an S-wave phase. This experiment searches for a sign change in the superconducting gap. (a) A ZBCP is seen for pure YBCO, as expected, since it has a D-wave gap. (b) No ZBCP is seen for $(X, Y) = (0.32, 0.32)$, suggesting it has an S-wave gap. These curves are representative of several measurements on each sample.

C. Evolution of the low-temperature penetration depth

The third experiment searched for nodes in the superconducting gap by the measuring the evolution of the superconducting penetration depth, λ, as a function of temperature, T. A D-wave gap has nodes leading to $\lambda \sim T$. An S-wave superconductor in the London limit (short coherence length) has $\lambda \sim T^2$ because it does not have nodes [6].

Figure 4 shows the changes in inductance, L, of a pancake coil placed on top of (X, Y) samples for $(X, Y) = (0, 0)$, $(0.13, 0)$, $(0.36, 0.16)$, and $(0.32, 0.32)$. Changes in L are proportional to changes in the superconducting penetration depth, λ [11]. The $(0, 0)$ and $(0.13, 0)$ are known D-wave gap materials. Hence, we expect that their L changes linearly with T, as observed. We find $L \sim T^2$ for $(0.36, 0.16)$ and $(0.26, 0.26)$ leading to $\lambda \sim T^2$ for both samples, as expected for an S-wave gap superconductor.

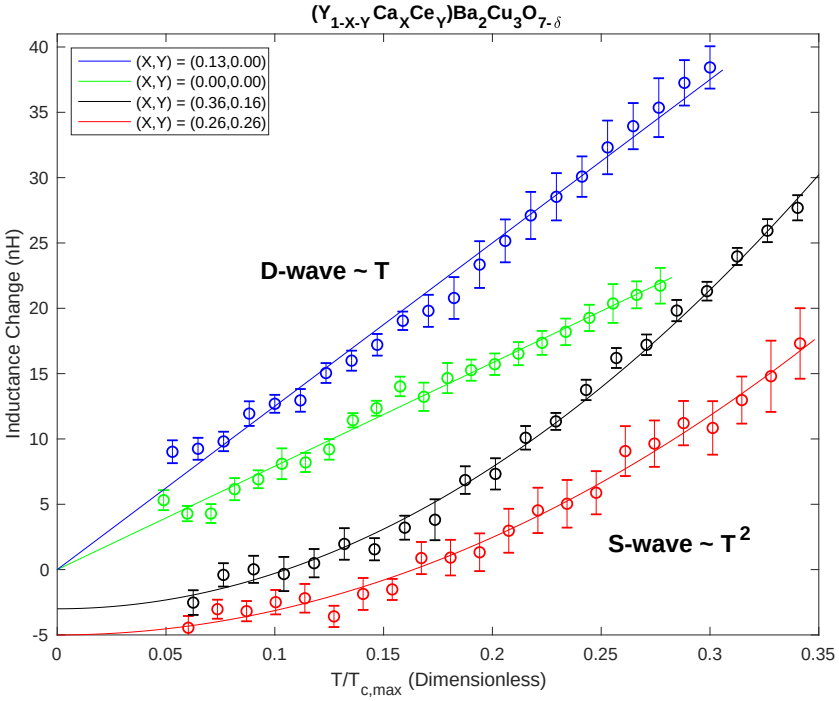

Fig. 4 | Evolution of the measured superconducting penetration depth change as a function of the normalized temperature, as seen by the change in inductance. The figure shows the change in inductance for two known D-wave gap phases, pure YBCO, $(X, Y) = (0, 0)$ (green), $(X, Y) = (0.13, 0.0)$ (blue), and two phases with $(X, Y) = (0.36, 0.16)$ (black) and $(0.26, 0.26)$ (red). For clarity, the black data are shifted downward by 3 nH and the red data are shifted downward by 5 nH. The data points are the measured inductance with $\pm 3\sigma$ error bars. The x-axis is the ratio $T/T_{c,max}$ where $T_{c,max}$ is the maximum superconducting temperature from Figure 2. For all curves, the change in inductance was measured from 4 K to 26 K. In the Supplement [11], we show that the measured change in inductance is proportional to the change in penetration depth of the superconducting sample, and also estimate many sources of errors in this measurement. The extrapolated $T = 0$ K inductance values are 19.276 μH, 20.623 μH, 20.349 μH, and 21.243 μH for $(0, 0)$, $(0.13, 0)$, $(0.36, 0.16)$, and $(0.26, 0.26)$, respectively. The solid blue and green curves are linear in T fits and the black and red curves are T^2 fits to the data. A linear T evolution of the penetration depth is expected for a D-wave gap and T^2 is expected for an S-wave gap. The green and blue curves show that YBCO with $(X, Y) = (0.0, 0.0)$ and $(0.13, 0.0)$ are D-wave, as expected. The black and red curves suggest that $(X, Y) = (0.36, 0.16)$ and $(0.26, 0.26)$ are S-wave gap phases of YBCO.

The changes in L in Figure 4 are several 10s of nanoHenrys. The magnitude of the extrapolated L at $T = 0$ is ≈ 20 μH for the four curves. A 1 nH change is a relative L change of $\sim 5 \times 10^{-5}$, making this experiment the most difficult of the three experiments in Figures 2, 3, and 4. A detailed description of this experiment and estimates of many potential errors is in the Supplement [11].

A possible D-wave gap explanation for $\lambda \sim T^2$ exists. Hirschfeld et al. [2] showed that a D-wave superconductor with non-magnetic impurities can lead to $\lambda \sim T^2$ for $T < T^*$, where T^* depends on the magnitude of single impurity scattering (in our case, a single Ca or Ce atom) and the ratio of $T_{c,max}$ for (X,Y) to $T_{c,max}$ for $(0, 0)$ (pure YBCO). For $T > T^*$, the theory predicts $\lambda \sim T$. Since Ca and Ce impurities reside at the Y site in YBCO and this site is not in the CuO_2 planes, where most of the density of the metallic band is located, the magnitude of single impurity scattering is small [17]. Extended Data Figure 4 shows that the theory prediction [2] for weak (Born) scattering plus the $T_{c,max}$ values measured in Figure 2 lead to the conclusion that $T^* \ll 1$ K for our experiment. Hence, a D-wave superconductor with impurity scattering does not explain the observed $\lambda \sim T^2$ up to 26 K as seen for $(0.36, 0.16)$ and $(0.26, 0.26)$.

D. Summary of the three experiments

Table I summarizes the findings from the three experiments in Figures 2, 3, and 4. In all three experiments, the results favored a crossover from a D-wave gap at low counter-doping to an S-wave gap at high counter-doping. These results imply that Figure 1b is correct—a technologically useful S-wave superconducting gap YBCO phase resides at ~ 70 K in YBCO heavily counter-doped with Ca and Ce impurities.

We found two papers in the literature where a crossover from D-wave superconductivity to S-wave was seen. First, in 2001, Yeh et al. [18] observed a $d + s$ superconducting gap symmetry for highly doped $(Y_{0.7}Ca_{0.3})Ba_2Cu_3O_{7-\delta}$ with $T_c = 78 \pm 2$ K. In our notation, this sample has $(X, Y) = (0.3, 0.0)$. From Figure 2, the T_c measured by Yeh et al., falls on the blue line for $T_{c,max}$ and is in the crossover region between a D-wave gap to an S-wave gap.

Second, in 2012, Reid et al. [19] found a crossover from a D-wave superconducting gap in the iron-pnictide KFe_2As_2 to an S-wave gap in $(Ba_{0.6}K_{0.4})Fe_2As_2$. The authors of this paper attribute the gap symmetry change to a change in the Fermi surface and Fermi level between the two pnictide samples. In our samples, we believe the gap symmetry has changed without altering the Fermi surface or the Fermi level.

Table I | Summary of the results of thre experiments on the gap symmetry. All three experiments suggest that Ca and Ce doped YBCO has changed from D-wave to an S-wave phase at high Ca and Ce counter-doping.

Figure	Physical Property	Experiment	Expected for D-wave	Expected for S-wave	Result
2	Superconducting gap magnitude	T_c change with non-magnetic counter-doping	T_c decreases with increasing counter-doping	T_c weakly dependent on counter-doping	S-wave
3	Superconducting gap phase	Point-Contact-Andreev-Reflection (PCAR)	Zero-Bias Conductance Peak (ZBCP)	No ZBCP	S-wave
4	Superconducting zero-energy excitations	Penetration depth, λ, dependence at low temperature, T	$\lambda \sim T$	$\lambda \sim T^2$	S-wave

II. CONCLUSIONS

The intent of this paper was to search for an S-wave gap symmetry YBCO phase beneath the known D-wave gap YBCO phase at ~ 90 K and determine its superconducting transition temperature. Our conjecture was that an S-wave YBCO phase was at ~ 70 K, and if true, will have huge implications for making high-field magnets using poly-crystalline superconducting wires. To test this conjecture, we counter-doped YBCO with Ca and Ce impurities, performed three experiments to study the superconducting gap symmetry, and found evidence suggesting that an S-wave gap symmetry phase does exist at ~ 70 K in all three experiments (see Table I).

A potential S-wave gap symmetry crossover in Ca and Ce counter-doped cuprate, $YBa_2Cu_4O_8$ (Y124) should be studied. Y124 is a stoichiometric crystal that is much more three-dimensional than YBCO (vastly improved conduction normal to its CuO_2 plane compared to YBCO). Y124 is intrinsically underdoped. Doping with 0.1 Ca brings Y124 up to optimal doping (highest T_c). Hence, counter-doping with 0.1 more Ca than Ce is desired for the highest T_c.

Poly-crystalline counter-doped wires of Y124 will be mechanically strong. Using the metallic precursor method [21] to form poly-crystalline wires of Y124 is already known to lead to grain alignments $< 10^o$ normal to the CuO_2 planes and grain alignments $< 15^o$ in the planes. While these grain mis-alignments made D-wave poly-crystalline Y124 impractical, a counter-doped Y124 that becomes S-wave may have a very large supercurrent density using this mature manufacturing process.

The results in this paper were obtained on poly-crystalline counter-doped samples. Ideally, one would like to repeat these experiments and additional experiments on single-crystals. The change in critical current density as a function of grain misalignment should also be measured to determine how much supercurrent can be transported in poly-crystalline wires.

Poly-crystalline wires should be synthesized and characterized. Two methods exist for making poly-crystalline wires from cuprates: Powder-in-Tube [22–24] and metallic precursors [21, 25–27]. If there is a large improvement in the supercurrent carrying ability of these wires, then an enormous opportunity exists for creating new and useful practical wires for high-magnetic field applications on a short timescale.

[1] Larbelestier, D., et al. *High-Tc superconducting materials for electric power applications.* Nature **414**, 368–377 (2001)

[2] Hirschfeld, P. and Goldenfeld, N. *Effect of strong scattering on the low-temperature penetration depth of a d-wave superconductor.* Physical Review B **48**, 4219–4222 (1993).

[3] Abrikosov, A. A. and Gor'kov, L. P. *Contribution to the Theory of Superconducting Alloys with Paramagnetic Impurities.* Soviet Physics–JETP **12**, 1243–1253 (1961).

[4] Anderson, P. W. *Theory of dirty superconductors* Journal of Physics and Chemistry of Solids **11**, 26–30 (1959)

[5] Tahir-Kheli, J. *Latent Room-Temperature T_c in Cuprate Superconductors.* arxiv:1702.05001 (2017).

[6] Tinkham, M. *Introduction to Superconductivity: Second Edition.* Dover Publications, page 104, (2004).

[7] Williams, G. V. M. et al. *NMR studies of overdoped* $Y_{1-x}Ca_xBa_2Cu_3O_{7-\delta}$. Physical Review B **57**, 8696–8701 (1998).

[8] Naqib, S. H. et al. *Temperature dependence of electrical resistivity of high-t-c cuprates - from pseudogap to overdoped regions.* Physica C-Superconductivity and Its Applications **387**, 365–372 (2003).

[9] Jin, S. et al. *Superconducting properties of* $YBa_2Cu_3O_{7-\delta}$ *with partial rare earth substitution.* Physica C: Superconductivity **173**, 75–79 (1991).

[10] Tallon, J. L. et al. *Generic superconducting phase behavior in high-T_c cuprates: T_c variation with hole concentration in* $YBa_2Cu_3O_{7-\delta}$. Physical Review B **51**, 12911–12914 (1995).

[11] *Supplemental Material.* See Supplemental Material for further details.

[12] Presland, M. R. et al. *General trends in oxygen stoichiometry effects on T_c in Bi and Tl superconductors.* Physica C: Superconductivity **176**, 95–105 (1991).

[13] Obertelli, S. D. et al. *Systematics in the thermoelectric power of high-T_c oxides.* Physical Revew B **46**, 14928–14931 (1992).

[14] Blonder, G. E. et al. *Transition from metallic to tunneling regimes in superconducting microconstrictions: Excess current, charge imbalance, and supercurrent conversion.* Physical Review B **25**, 4515–4532 (1982).

[15] Tanaka, Y. and Kashiwaya, S. *Theory of Tunneling Spectroscopy of d-Wave Superconductors.* Physical Review Letters **74**, 3451–3454 (1995).

[16] Kashiwaya, S. et al. *Theory for tunneling spectroscopy of anisotropic superconductors.* Physical Review B **53**, 2667–2676 (1996).

[17] Alloul, H. et al. *Defects in correlated metals and superconductors.* Reviews of Modern Physics **81**, 45–108 (2009).

[18] Yeh, N. C. et al. *Evidence of Doping-Dependent Pairing Symmetry in Cuprate Superconductors.* Physical Review Letters **87** 087003 (4pp) (2001).

[19] Reid, J-Ph. et al. *From d-wave to s-wave pairing in the iron-pnictide superconductor (Ba,K)*Fe_2As_2. Superconductor Science and Technology **25**, 084013 (10pp) (2012).

[20] Soulen, R. J. et al. *Measuring the Spin Polarization of a Metal with a Superconducting Point Contact.* Science **282**, 85–88 (1998).
[21] Masur, L.J. et al. *Bi-axial texture in $Ca_{0.1}Y_{0.9}Ba_2Cu_4O_8$ composite wires made by metallic precursors.* Physica C: Superconductivity **230**, 274–282 (1994).
[22] Zhang, Z. et al. *Investigation of the melt-growth process of $YbBa_2Cu_3O_{7-\delta}$ powder in Ag-sheathed tapes.* CrystEngComm **21**, 1369–1377 (2019).
[23] Paturi, P. et al. *Texture of YBCO/Ag PIT-tapes.* Physica C: Superconductivity **408-410**, 935–936.
[24] Chaffron, L. and Régnier, P. *Present state of our research on silver sheathed REBa2Cu3O7 superconductors.* Superconductor Science and Technology **4**, S247–S249 (1991).
[25] Otto, A. et al. *Properties of high-T_c wires made by the metallic precursor process.* JOM **45**, 48–52 (1993).
[26] Otto, A. et al. *Multifilamentary Bi-2223 composite tapes made by a metallic precursor route.* IEEE Transactions on Applied Superconductivity **3** 915–922 (1993).
[27] Otto, A. et al. *Progress towards a long length metallic precursor process for multifilament Bi-2223 composite superconductors.* IEEE Transactions on Applied Superconductivity **5** 1154–1157 (1995).
[28] Hardy, W. N., et al. *Precision measurements of the temperature dependence of λ in $YBa_2Cu_3O_{6.95}$: Strong evidence for nodes in the gap function.* Physical Review Letters **70**, 3999–4002 (1993).

EXTENDED DATA FIGURES

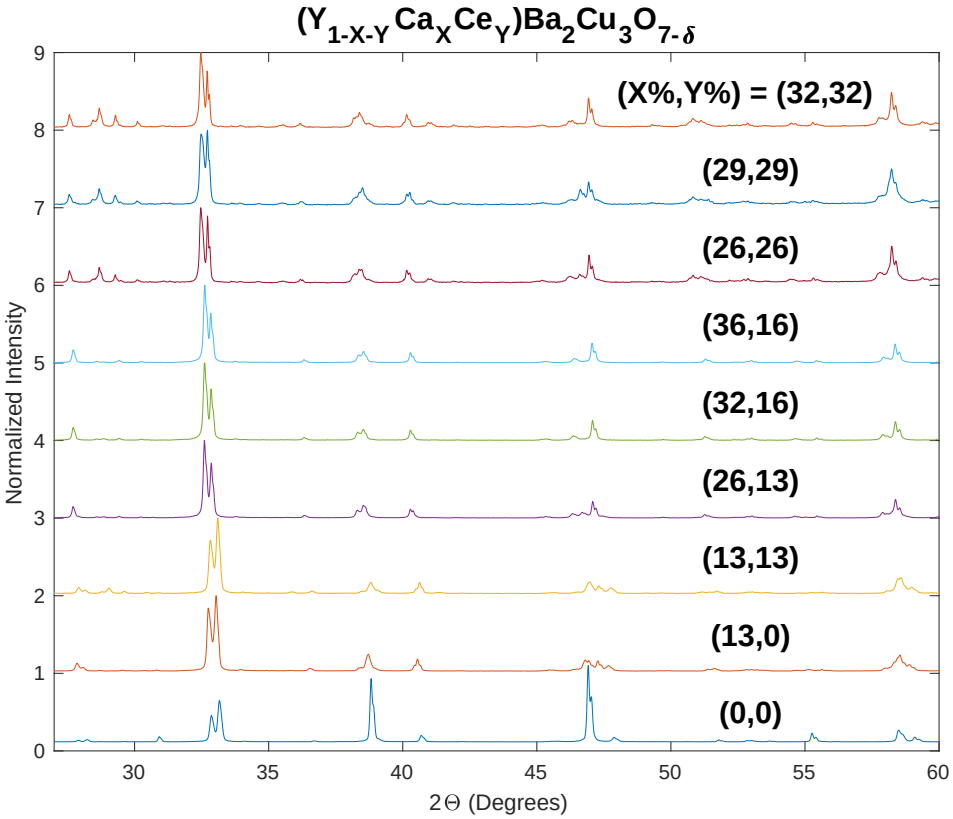

Ext. Data Fig. 1 | X-ray diffraction (XRD) patterns for $(Y_{1-x-y}Ca_xCe_y)Ba_2Cu_3O_{7-\delta}$ [hereinafter, denoted (X,Y)] for (X,Y) ranging from pure YBCO, or (X,Y) = (0,0), up to (X,Y)=(0.32, 0.32). There is a small amount of alien phase seen below 30° for the three X = Y samples, (0.26, 0.26), (0.29, 0.29), and (0.32, 0.32). Otherwise, the samples are single-phase. See Extended Data Figures 2 and 3 and Extended Data Tables II and III.

Table II | Rietveld x-ray occupation of Ca and Ce atoms on Y for (X,Y) = (0.26, 0.13), (0.32, 0.16), and (0.36, 0.16). These results show that the Ca and Ce atoms have substituted onto the Y site and that the measured composition is close to the desired composition.

	(0.26, 0.13)		(0.32, 0.16)		(0.36, 0.16)	
Element	Expected	Refined	Expected	Refined	Expected	Refined
Y	0.61	0.61	0.52	0.52	0.48	0.48
Ca	0.26	0.255(4)	0.32	0.300(4)	0.36	0.348(3)
Ce	0.13	0.135(4)	0.16	0.180(4)	0.16	0.172(3)
Ba	2	2	2	2	2	2
Cu	3	3	3	3	3	3
O	7	7	7	7	7	7

Table III | Phase composition of (X,Y) = (0.26, 0.13), (0.32, 0.16), and (0.36, 0.16) in weight % as determined by Rietveld x-ray diffraction. In these samples, the alien phase is $BaCuO_2$.

	Phase Composition (weight %)		
	(0.26, 0.13)	(0.32, 0.16)	(0.36, 0.16)
$(YCaCe)Ba_2Cu_3O_{7-\delta}$	98.3(6)	98.3(6)	97.1(5)
$BaCuO_2$	1.66(6)	1.67(6)	2.85(5)

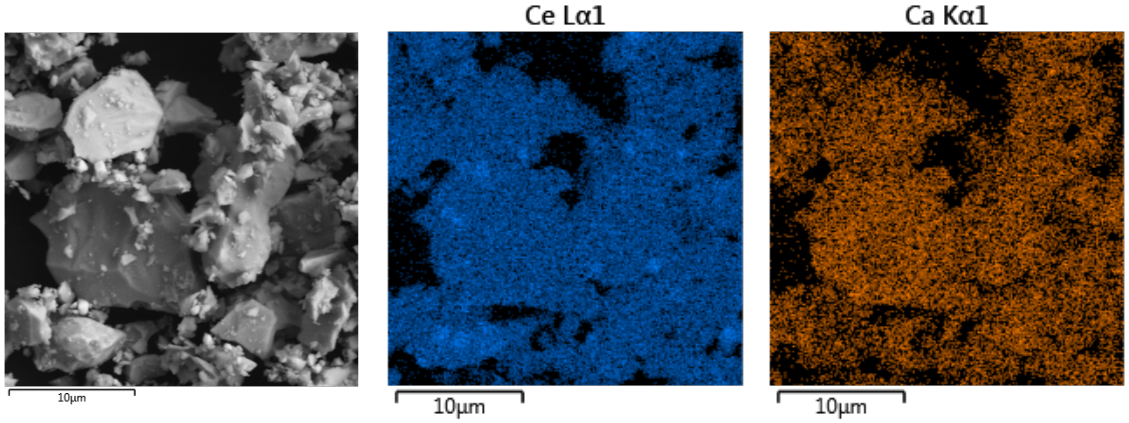

Ext. Data Fig. 2 | Back-scattered scanning-electron-microscopy (BSE-SEM) and energy-dispersive X-ray (EDX) analysis of (X,Y) = (0.26, 0.26). The BSE-SEM picture on the left shows no significant contrast differences that would suggest large grains of secondary phases. The Ce Lα1 and Ca Kα1 EDX distributions in the two right figures show that Ca and Ce are dispersed throughout the sample with similar distributions. This similarity implies that the grains have X $\approx$ Y. This finding is important in order to verify that the "saturation" of the T_c values on the right-hand side of Figure 2 are not due to an incorrect assignment of the (X, Y) values of the sample.

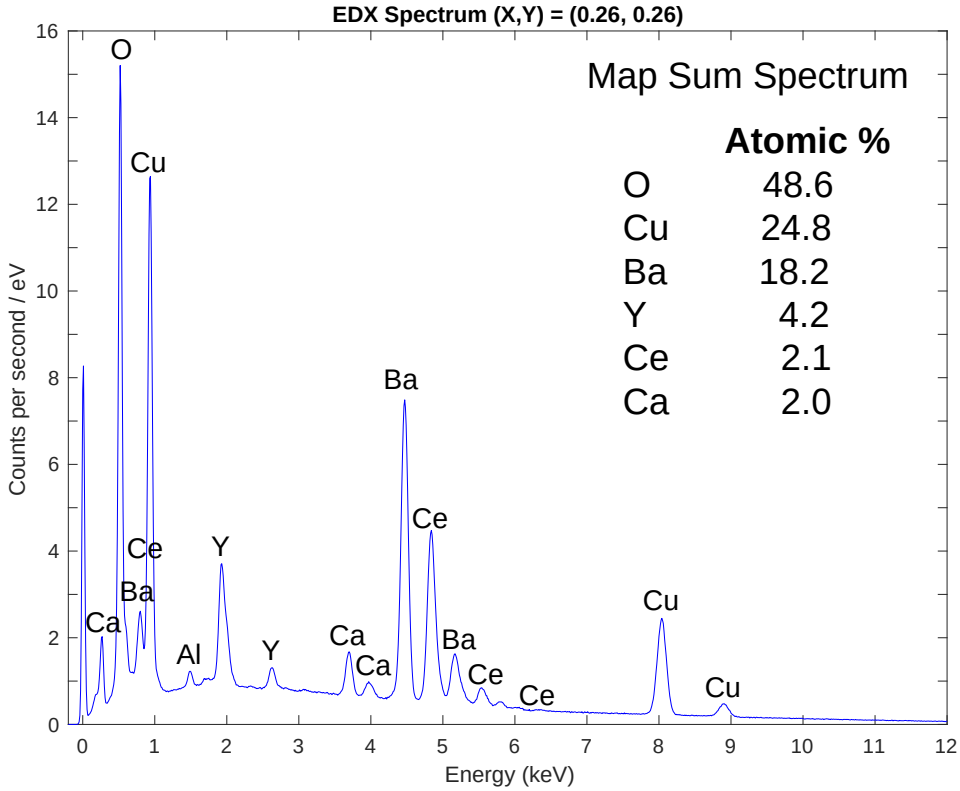

Ext. Data Fig. 3 | EDX mass sum spectrum of an (X,Y) = (0.26, 0.26) sample. The atomic % of each element is shown in the inset. From these values, we infer that Ca : Ce = 1 : 1, Ca : Y = 1 : 2, and (Y, Ca, Ce) : Ba : Cu : O = 1 : 2 : 3 : 6 within experimental error. Hence, the synthesized $(X, Y) = (0.26, 0.26)$ sample is close to the desired starting composition. This figure combined with Extended Figure 2 shows that the "saturation" of T_c in Figure 2 extends over a broad counter-doping range, as expected for an S-wave YBCO phase. The plot shows the spectrum up to 12 keV. The data was taken up to 15 keV. There were no large peaks above 12 keV. The large peak at 0 keV is the instrumental response and does not correspond to any element. The Al peak at $\approx$ 1.5 keV is due to the sample holder.

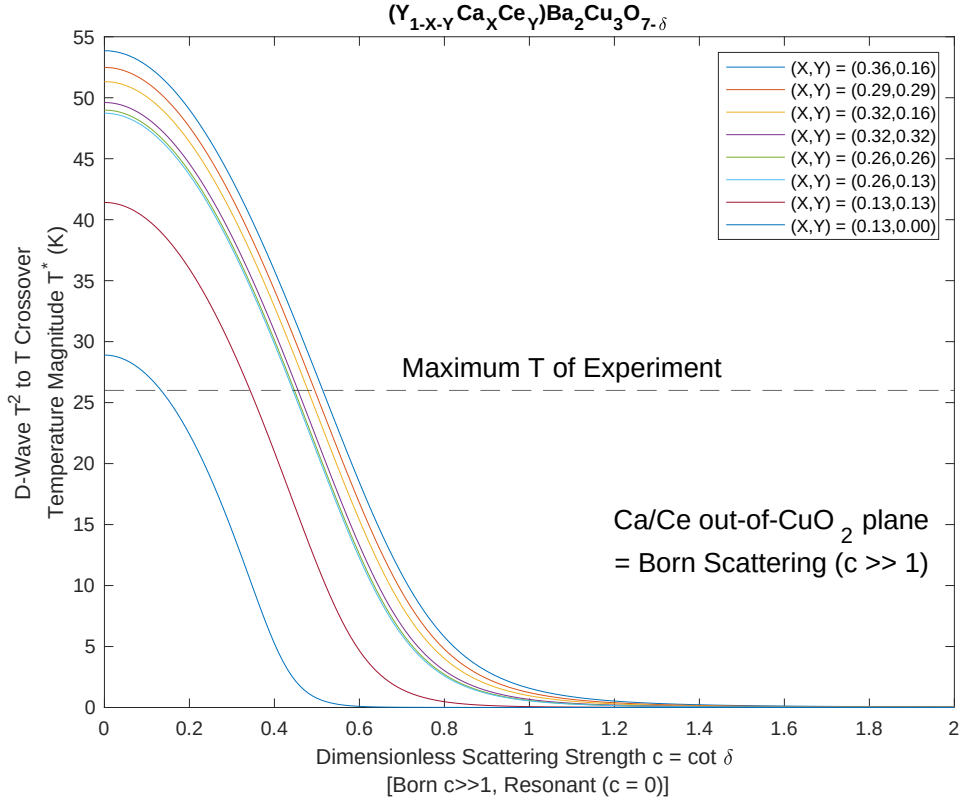

Ext. Data Fig. 4 | Theoretical calculation of the temperature, T^*, for the crossover from a $\lambda \sim T^2$ penetration depth for $T < T^*$ and a linear $\lambda \sim T$ for $T > T^*$ as a function of c, the cotangent of the scattering phase shift, δ, per impurity (Ca or Ce) arising from non-magnetic counter-doping in a D-wave superconductor. Non-magnetic impurity scattering in a D-wave superconductor leads to $\lambda \sim T^2$ for $T < T^*$ because it creates a residual density of states for excitations at zero-energy. The curves in this figure are calculated from the theory of Hirschfeld and Goldenfeld [2] using the T_c values measured in Figure 2. For each c value and the ratio of T_c for sample (X, Y) to the T_c of pure YBCO, the crossover temperature T^* is calculated. The horizontal line at 26 K in the figure is the maximum temperature of the penetration depth experiment. Since $\lambda \sim T^2$ for the $(0.36, 0.16)$ and $(0.26, 0.26)$ samples all the way up to the maximum temperature of the experiment, the largest possible scattering strength is $c \approx 0.55$ in order that $T^* > 26$ K. Since the Ca and Ce atoms substitute at Y sites that reside out of the CuO_2 planes in YBCO, the scattering is weak (Born) scattering [17]. Born scattering implies $c \gg 1$. Hence, the observed $\lambda \sim T^2$ for $(0.36, 0.16)$ and $(0.26, 0.26)$ cannot be explained by non-magnetic impurity scattering of D-wave counter-doped YBCO. Therefore, the penetration depth experiment in Figure 4 suggests an S-wave YBCO phase at high Ca and Ce counter-doping.

METHODS

Materials Synthesis

The following chemicals were used for the synthesis of all the cuprate precursors: $BaCO_3$ (99.8% purity), Y_2O_3 (99.99%), CuO (99.9%), CeO_2 (99.9%), and $CaCO_3$ (99.8%). The initial powders were mixed and homogenized in elemental ratios. Precursor powders were prepared by conventional multi-step solid-state reaction. The raw materials were mixed together and calcined in batches of several hundreds of grams. The calcination of YBCO-123 precursors were done in five steps at temperatures of 850 C, 870 C, 880 C, 890 C and 910 C with intermediate homogenization. Calcination of the counter-doped (Ca/Ce - YBCO) precursors had to be optimized to ensure correct phase formation and to avoid any liquid phase (Ba-Cu-O) loss. The final process was a function of the doping level. In all cases they include 2 low temperature calcinations in a powder form (850 C, 870 C), two calcinations in pre-pressed form (890 C, 910 C; 40g pellets, diameter 28 mm, uniaxial pressing) and several sinterings at 910 C (40g pellets, diameter 28 mm, uniaxial pressing + cold isostatic pressing). The progress of calcination was monitored by x-ray diffraction (XRD) to obtain maximal phase purity, as shown in Extended Table III. An x-ray Rietveld analysis was performed on $(Y_{1-x-y}Ca_xCe_y)Ba_2Cu_3O_{7-\delta}$ with (X,Y) = (0.26, 0.13) and (0.32, 0.16) to ensure that the Ca and Ce atoms substituted onto the Y sites (see Extended Table II).

For the (0.26, 0.26), (0.29, 0.29), and (0.32, 0.32) samples, raw materials were mixed into a batch of 1 kg and milled using a vibratory disc mill. First, the powder was calcined at 850 C and 870 C, with a temperature ramp of 12h and a hold of 72h at ambient atmosphere. The powder was then uniaxially pressed into pellets (40g, 32mm diameter) with a force of 6 tons and subsequently pressed isostatically at 300 MPa. The pellets were sintered 4 times (once at 890 C and 3 times at 910 C with a ramp of 12h and hold of 48h for all sintering cycles). The pellets were crushed and milled between the sintering cycles to achieve high homogeneity, followed by the same pressing process.

BSE-SEM and EDS were performed on the (0.26, 0.26) sample. The morphology was investigated using SEM with a FEG electron source (Tescan Lyra dual beam microscope, TESCAN Brno, s.r.o.). Elemental composition and mapping were performed using an EDS analyzer (X-MaxN) with a 20 mm^2 SDD detector (Oxford Instruments, High Wycombe, UK) and AZtecEnergy software. Elemental maps were measured 5 times with an acquisition time of 100 sec. To conduct the measurements, the samples were placed on a carbon conductive tape and a BSE detector was used to obtain the SEM photography. The acquisition time for each photograph was set to 22 sec. SEM and SEM-EDS measurements were carried out using a 15 kV electron beam. These measurements were done on several

locations with magnification from 5,000x to 30,000x, yielding the same data regardless of the location and magnification.

Poly-crystalline cylindrical $(Y_{1-x-y}Ca_xCe_y)Ba_2Cu_3O_{7-\delta}$ pellets with diameter 15 mm and height 6 mm for (X,Y) = (0.0, 0.0), (0.13, 0.0), (0.13, 0.13), (0.26, 0.13), (0.32, 0.16), (0.36, 0.16), (0.26, 0.26), (0.29, 0.29), and (0.32, 0.32) were synthesized. Further annealing at low temperatures (T < 400 C) was performed in the gases Air, Oxygen, Ozone, Argon, and Hydrogen in order to change the doping in the grains and grain boundaries. Over 60 different anneals were performed on over 100 samples during the course of this work. The length of the anneals varied from a few hours to several weeks. We found that every single sample we checked had a superconducting transition. This observation shows that superconductivity in Ca and Ce doped $(Y_{1-x-y}Ca_xCe_y)Ba_2Cu_3O_{7-\delta}$ is remarkably robust. The room-temperature thermopower was measured for each pellet after the low-temperature anneals to determine the CuO_2 plane hole doping level by applying the thermopower relation between thermopower and doping discovered by Tallon et al. [12, 13]. We found the maximum T_c occurs at the thermopower ($\approx +2$ μV/K) predicted by this relation.

Description of the Experiments

The superconducting transition temperature, T_c, and the temperature dependence of the penetration depth, λ, were measured by the change in inductance of a coil placed on the sample at a fixed frequency of 500 kHz. For the T_c values in Figure 2, we made a 40-turn pancake coil with inner diameter of 5 mm and outer diameter of 8 mm. For λ shown in Figure 4, we made a 100-turn pancake coil with inner diameter of 5 mm and outer diameter of 15 mm. The room-temperature inductance of the 40-turn and 100-turn coils at 100 kHz is 9.9 μH and 81.9 μH, respectively.

Both coils are made from non-magnetic Phosphor-Bronze (CuSnP alloy) magnet wire with diameter 150 μm. We used Phosphor-Bronze because it has a large resistivity (~ 8.9 $\mu\Omega$-cm) that changes less than 0.2 % from zero-temperature up to 26 K. Its skin depth at 500 kHz is ~ 225 μm. The skin-depth is larger than the diameter of the wire. Hence, changes in the coil inductance due temperature dependent skin-depth changes can be neglected.

There is a redistribution of the current density in the cross-section of the wire due to the proximity effect arising from the diamagnetic screening currents in the superconducting sample. This effect pulls the current distribution in the coil wire towards the sample. We find that it increases the coil resistance by ~ 80 % between the normal state and the low temperature superconducting state leading to a $\sim 1 - (1/1.8) = 44$ % reduction in the cross-sectional area of the Phosphor-Bronze wire that carries current. The important point is that, while this current distribution is different from the normal state current distribution, it changes the derivative of the coil self-inductance with penetration depth, $dL/d\lambda$, negligibly over the temperature range of the λ experiment [11]. Hence, it does not change the shape of the L curves in Figure 4.

A Cu block with resistive heating elements inside was mounted on the cold head using Silver paste as the thermal contact. A Cernox^{TM} semiconducting thermometer was mounted on the Cu block. The samples were pressed onto the Cu block using Apiezon-N grease.

The coil was kept in contact with the sample by the force from two small springs. The force from the springs was adjusted such that there was enough force to keep the coil on the sample while maintaining a small enough coil-to-sample force so that the thermal resistance between the coil and sample was large. This adjustment reduces uncertainties in the sample temperature arising from its contact with the coil that may be at a different temperature. Estimates of the thermal diffusivity of the samples and the thermal resistance between the coil and sample can be found in the Supplement [11].

All our quoted T_c values are the onset T_c rather than the midpoint T_c because T_c(onset) was more consistent with the measured room-temperature thermopower. T_c(midpoint) was found to be sensitive to the nature of the low temperature annealing. Hence, the results in Figure 2 are the maximum onset T_c for each (X,Y) = (Ca,Ce) doping.

In Figure 4, the change in inductance, L, with temperature is plotted rather than the change in λ with temperature because the constant derivative, $dL/d\lambda$, is known only approximately due to uncertainties in the coil-to-sample distance. Since the shape of the change in L is the same as the shape of the change in λ, the gap symmetry question can be answered without knowing $dL/d\lambda$. From microwave measurements of the change in the penetration depth [28] of YBCO and the corresponding data in Figure 4, $dL/d\lambda \approx 2.0$ nH/nm. A schematic of the experiment and the details of the method to extract the coil L from reflection coefficient measurements is in the Supplement [11].

The change in the penetration depth (measured as a change in inductance, L) was obtained for many samples. The L was measured as the sample was cooled down from 26 K to 4 K and then reheated back to 26 K. If the hysteresis in L was large, the run was rejected. The quoted L values average the cool down and warm up sweeps. Most of these samples had changes in inductance over the temperature range of $4 - 26$ K that was a few times larger than the ~ 20 nH change found for pure $YBa_2Cu_3O_{7-\delta}$ (see Figure 4). These samples were also rejected, despite having relatively sharp T_c transitions, because it was possible that a small fraction of grains inside the sample had $T_c < 26$ K, leading to an increase in inductance with temperature due to superconductor-normal phase transitions during the experiment.

The two additional issues that could affect the measurement are coil heating and the effect of the temperature dependence of the critical-current density of the Josephson junctions formed at the grain boundaries, J_c(Josephson). These two effects may lead to non-intrinsic temperature changes in the total inductance. All λ experiments were done at transmit power of -40 dBm $= 0.1$ μW. Approximately half of this power was absorbed and the remainder was reflected back to the Vector Network Analyzer (VNA). Additional experiments were run at -50 dBm $= 0.01$ μW and -30 dBm $= 1$ μW. No change in the measured inductance was found between the -40 dBm and -50 dBm runs, indicating that the superconducting shielding currents in the sample were less than J_c(Josephson) and that there was negligible coil heating. The Supplement [11] estimates possible errors. The Supplement [11] also describes the data acquisition with the VNA and our procedure for calculating the error bars for L in Figure 4.

The Point-Contact-Andreev-Reflection (PCAR) data were obtained using a Cu tip that was attached to a rod driven by a micrometer. Measurements of the current-voltage (I-V) and differential conductance (dI/dV) characteristics were made using a conventional four-terminal probe arrangement with the conductance data obtained using a standard ac lock-in technique at a frequency of 10 kHz. The point contacts and samples were immersed in a liquid helium bath at 4.2 K. Further details of the measurement technique can be found in reference [20].

ACKNOWLEDGMENTS

We thank Thomas E. Sutto for suggesting Ce as a potential +4 oxidation state impurity atom that will reside at the Y site. This work was partially funded by the Office of Naval Research under Contract Number N00014-18-1-2679.

COMPETING INTERESTS

The authors declare they have no competing financial interests.

AUTHOR CONTRIBUTIONS

J.T.-K. and C.A.M. conceived the project and designed experiments for thermopower and transition temperature. J.T.-K performed the room-temperature thermopower measurements, devised and performed the penetration depth experiments, devised the coax-correction and current-distribution correction protocols described in the supplement, and did all the theory calculations. Additional annealing at lower temperatures was done by J.T.-K. and C.A.M. They also wrote the paper. T.H. synthesized the materials and contributed to the interpretation of the XRD, SEM, and EDX data. M.L. performed the XRD, SEM, and EDX measurements, and did the materials characterization. M.L. also contributed to the materials characterization between sinters. M.S.O. designed and performed the PCAR experiment.

CORRESPONDENCE

Correspondence and requests for materials should be addressed to J.T.-K. (email: jamil@caltech.edu).